Biophysical Journal
Article

Biophysical Society

Interleaflet organization of membrane nanodomains: What can(not) be resolved by FRET?

Barbora Chmelová,[1,2] David Davidović,[1,3] and Radek Šachl[1,*]
[1]J. Heyrovský Institute of Physical Chemistry of the Czech Academy of Sciences, Prague, Czech Republic; [2]Faculty of Mathematics and Physics, Charles University, Prague, Czech Republic; and [3]Department of Physical and Macromolecular Chemistry, Faculty of Science, Charles University, Prague, Czech Republic

ABSTRACT Plasma membranes as well as their simplified model systems show an inherent nanoscale heterogeneity. As a result of strong interleaflet interactions, these nanoheterogeneities (called here lipid nanodomains) can be found in perfect registration (i.e., nanodomains in the inner leaflet are registered with the nanodomains in the outer leaflet). Alternatively, they might be interleaflet independent, antiregistered, or located asymmetrically in one bilayer leaflet only. To distinguish these scenarios from each other appears to be an experimental challenge. In this work, we analyzed the potential of Förster resonance energy transfer to characterize interleaflet organization of nanodomains. We generated in silico time-resolved fluorescence decays for a large set of virtual as well as real donor/acceptor pairs distributed over the bilayer containing registered, independent, antiregistered, or asymmetrically distributed nanodomains. In this way, we were able to identify conditions that gave satisfactory or unsatisfactory resolution. Overall, Förster resonance energy transfer appears as a robust method that, when using donor/acceptor pairs with good characteristics, yields otherwise difficult-to-reach characteristics of membrane lipid nanodomains.

SIGNIFICANCE This work first explores the potential of Förster resonance energy transfer (FRET) to characterize interleaflet nanodomain coupling and then shows how a FRET experiment can be designed to achieve optimal resolution toward nanodomain coupling. Importantly, the analysis identifies as the most critical the following parameters fundamentally affecting the resolution of FRET: the Förster radius and its value related to the interlayer distance at which donors and acceptors in the opposing membrane leaflets are separated from each other and the donor and acceptor partition coefficients characterizing their distribution between the domain and nondomain region. By setting these parameters correctly, FRET allows for the characterization of interleaflet nanodomain organization with unprecedented detail.

INTRODUCTION

The ongoing intensive research of the organization of plasma membranes suggests that they are nanoscopically heterogeneous both in their structure and chemical composition (1–5). Up to now, the formation of membrane heterogeneities, known in literature as lipid nanodomains, has been observed not only in cellular membranes but also in their synthetic models, comprising supported phospholipid bilayers, free-standing membranes of giant unilamellar vesicles (GUVs) or other (multi)lamellar structures (2,6,7). These nanodomains exist even in lipid mixtures containing solely two distinct types of lipids (8). Although the nanodomains have been characterized so far by diverse experimental approaches (9), their features and importance for membrane-related biological functions are still mostly unknown.

Considering that plasma membranes consist of two lipid layers that are in close contact, it is quite likely that the nanodomains in one layer will affect the positions of the nanodomains in the other layer. In principle, the following hypothetical scenarios may arise (Fig. 1): 1) nanodomains are perfectly registered across the bilayer leaflets, meaning that the nanodomains in the inner leaflet occupy the same lateral positions as the nanodomains in the outer leaflet (Fig. 1 *A*); 2) the nanodomains exist in both leaflets and are fully independent of each other (Fig. 1 *B*); 3) nanodomains are antiregistered (Fig. 1 *C*), implying that the nanodomains in both leaflets avoid each other, and, thus, the nanodomains in the inner leaflet cannot occupy the lateral

Submitted June 9, 2022, and accepted for publication November 7, 2022.
*Correspondence: radek.sachl@jh-inst.cas.cz
Editor: Ilya Levental.
https://doi.org/10.1016/j.bpj.2022.11.014

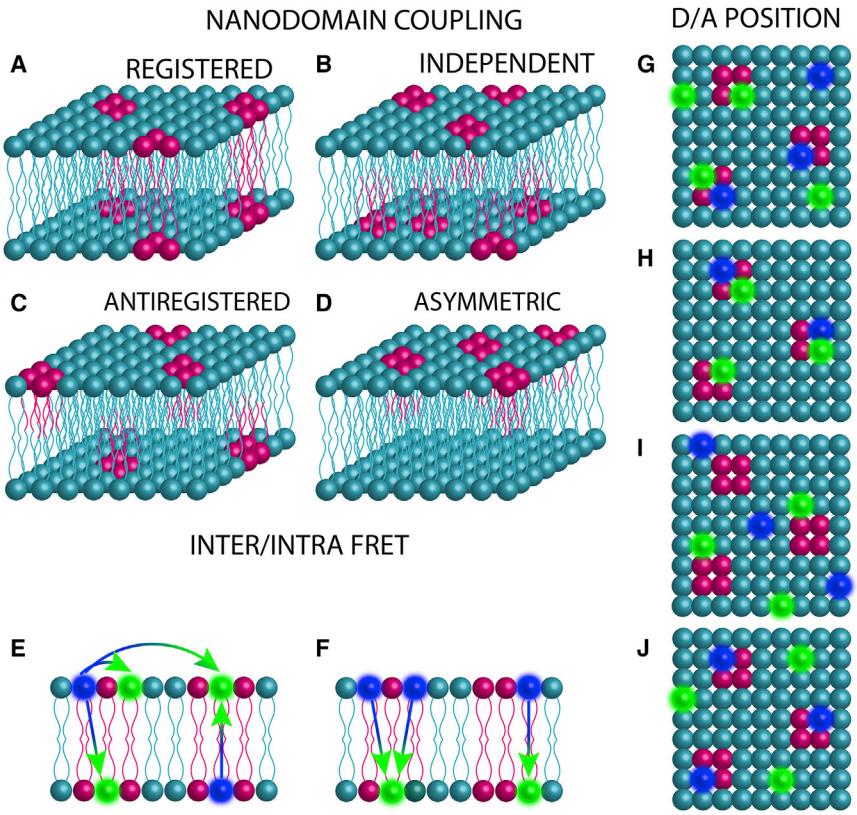

FIGURE 1 (*A–D*) Interleaflet organization of lipid nanodomains (depicted in *pink*): (*A*) registered (= interleaflet coupled), (*B*) interleaflet independent, or (*C*) antiregistered nanodomains or (*D*) nanodomains formed asymmetrically in one bilayer leaflet. (*E* and *F*) Distribution of D (*blue spheres*) and A (*green spheres*) with respect to both bilayer leaflets: (*E*) symmetric, where both intra- and inter-FRET processes occur and (*F*) asymmetric, where D and A occupy opposite leaflets. Under such circumstances, intra-FRET is eliminated, and only inter-FRET can take place. (*G–J*) Distribution of D and A relative to the nanodomains: (*G*) both D and A have equal affinity to nanodomains and the region outside of them corresponding to case 0, (*H*) both D and A have pronounced affinity to nanodomains ($K_D(D/A) > 1$; case I), (*I*) both D and A have low affinity to nanodomains ($K_D(D/A) < 1$; case II), and (J) Ds have increased affinity to nanodomains ($K_D(D) > 1$) whereas As are excluded from them ($K_D(A) < 1$; case III). To see this figure in color, go online.

For a Figure360 author presentation of Figure 1, see https://doi.org/10.1016/j.bpj.2022.11.014. Figure360▷

positions taken by the nanodomains in the outer leaflet, and vice versa; and 4) nanodomains are formed in an asymmetric manner in one leaflet only (Fig. 1 *D*). Due to the low thickness of the lipid bilayer at only a few nanometers and a small nanodomain size that is close to or below the resolution of optical microscopes, it is experimentally challenging to distinguish these possible scenarios from each other and thus to find out how nanodomains are organized between both bilayer leaflets.

Recently, we introduced a new fluorescence spectroscopy method Förster resonance energy transfer analyzed by Monte Carlo simulations (MC-FRET) for the characterization of interleaflet organization of lipid nanodomains and documented, in a few specific cases, that the nanodomains of variable sizes between 10 and 160 nm are perfectly registered across both leaflets (10–12). According to our knowledge, MC-FRET is the only, up to date, available experimental technique that can resolve interleaflets coupled from independent nanodomains in free-standing model lipid bilayers. Its applicability to the plasma membranes of living cells will need to be tested in the future.

The resolution of this method hangs on several parameters (8,13,14). In particular, it depends on the intrinsic properties of the chosen donor (D)-acceptor (A) pair, including the affinity of D and A to the nanodomains (characterized by their partition coefficient K_D(D/A)), their Förster radius, the distance between the D and A planes, or the distribution of D and A between both leaflets (Fig. 1). Thus, not every D/A pair is suitable for the characterization of nanodomain coupling, and each of them has specific limits in what it can(not) resolve.

In this work, we employed MC simulations and generated time-resolved fluorescence decays for a large ensemble of virtual D/A pairs having various properties (see the paragraph above) as well as real D/A pairs that have already turned out to be useful in the characterization of membrane nanodomains. All of these pairs were distributed on the bilayers containing registered, independent, antiregistered, or asymmetrically distributed nanodomains. In this way, we could investigate the limits of FRET in the characterization of nanodomain coupling.

We show that despite the limited choice of suitable D/A pairs and their generally low affinity to the (non)domain region that decreases the resolution, the probe partition coefficients are high/low enough to allow for characterization of nanodomain organization in a broad range of nanodomain radii $R/R_0 \geq 2$ (R_0 denotes the Förster radius) and relative surface area occupied by nanodomains $area \geq 10\ \%$ with unprecedented detail. Care should be taken when choosing D/A pairs with a low Förster radius or when resolving independent from antiregistered nanodomains since low FRET resolution is expected in these cases. Importantly, the analysis identifies the relatively popular D/A pairs consisting of NBD-DPPE (D) and rhodamine-DOPE (A) or

Bodipy-FL-GM_1 (D) and Bodipy-564/570-GM_1 (A) as the most efficient ones.

MATERIALS AND METHODS

Methodology

Generation of time-resolved fluorescence decays by MC simulations

MC simulations were used in this work to simulate FRET in nanoscopically heterogeneous bilayers separated into two distinct regions: a domain and a nondomain region. By intention, we make no assumptions about the properties or composition of the domain and nondomain regions. The results of the simulations can thus be applied both to the case where the domains are more ordered than the surroundings (having, for instance, a liquid-ordered or gel character) or, conversely, to the situation where the surroundings are more ordered. In the simulations, the nanodomains were assumed to be circular in shape and uniform in size with the nanodomain radius $\langle R \rangle$. The nanodomains in both bilayer leaflets were generated to be 1) registered; 2) independent; 3) antiregistered; or 4) localized in one leaflet only, and D and A were distributed either symmetrically in both leaflets or asymmetrically in opposite bilayer leaflets (Fig. 1). The simulations were performed in the simulation box with dimensions of $10R_0 \times 10R_0$ and its eight copies mimicking periodic boundary conditions. The entire process is initiated with the generation of a defined number of nanodomains corresponding to the surface density $\langle area \rangle$ on the bilayer surface. In the next step, D and A are distributed between nanodomains and the remaining bilayer part according to their partition coefficient K_D(D) and K_D(A) at a D/A-to-lipid ratio of 1:200. Of note, the dependence of the FRET resolution on the A-to-lipid ratio is fairly flat between 1:200 and 1:1,000; thus, any value selected within this range guarantees a good FRET resolution (see Figure S3). R_0 is assumed to be constant in the domain and nondomain region. The K_D is defined as

$$K_D(D/A) = [D/A]_{inside} \Big/ [D/A]_{outside}, \quad (1)$$

where $[D/A_{inside}]$ and $[D/A_{outside}]$ denote D/A surface concentrations inside or outside of the nanodomains, respectively (13). Whereas Ds are located in the central box only at a probe-to-lipid ratio of 1:200, As are placed into all nine boxes at the same probe-to-lipid ratio to mimic the bilayers that are infinitely large. Then, a D is randomly excited, and the time at which energy transfer takes place is calculated. The overall energy transfer rate Ω_i modulates the process according to $\Delta t_i = -\ln \gamma / \Omega_i$, where γ is a randomly generated number between 0 and 1. The outcome of each simulation step is the time interval Δt_i between the excitation and energy transfer event. By constructing a histogram of Δt_i intervals, the total survival probability function $G(t)$ is obtained, and the simulated decay of D quenched by the A, $F_{DA}(t)$, is calculated: $F_{DA}(t) = G(t)F_D(t)$. Here, $F_D(t)$ denotes the experimentally recorded D decay in the absence of A, which may not necessarily be monoexponential (10,15). Unless otherwise stated, a biexponential decay of Bodipy-FL attached to the headgroup of ganglioside GM_1 was used as $F_D(t)$ that enters the simulations.

RESULTS AND DISCUSSION

Analyzing the resolution of FRET

MC-FRET has been developed to fit experimental time-resolved fluorescence decays of the Ds quenched by As with the decays generated by MC simulations (8,16). As we have shown by simulations and experiments (8,10), if fluorescent probes having increased or decreased affinity to lipid nanodomains are used in an MC-FRET experiment, the shape of recorded fluorescence decays will change depending on the size of nanodomains (characterized by their average nanodomain radius $\langle R \rangle$), their surface density $\langle area \rangle$, and, importantly, on the organization of nanodomains between both bilayer leaflets (Fig. 2). Consequently, varying the input simulation parameters $\langle R \rangle$ and $\langle area \rangle$ can be determined (10,17).

Moreover, thanks to the energy transfer that occurs from one leaflet to the other one, MC-FRET offers excellent axial resolution and can be used to discriminate between the following most likely scenarios that can occur in the membrane: 1) registered (Fig. 1 *A*), 2) interleaflet-independent (Fig. 1 *B*), and 3) antiregistered (Fig. 1 *C*) nanodomains and 4) nanodomains formed asymmetrically in one leaflet only (Fig. 1 *D*). The most probable scenario is identified by comparing the fits by means of χ^2 values for scenarios 1–4 (10).

The resolution of FRET can be characterized by "RES parameter"

In this work, we introduce a resolution parameter (RES), defined as

$$\mathrm{RES} = \frac{1}{n} \sum_{i=1}^{n} \frac{\left(F_{DA,SC1}(t_i) - F_{DA,SC2}(t_i)\right)^2}{F_{DA,SC1}(t_i)} 100, \quad (2)$$

which turns out to be helpful in the characterization FRET resolution toward nanodomain coupling. RES expresses the difference between the simulated fluorescence decay for registered/independent/antiregistered or asymmetrically distributed nanodomains, $F_{DA,SC1}(t)$, and the simulated decay for one of the three alternative scenarios (see Fig. 2 for a more thorough explanation of the RES parameter); furthermore, n corresponds to the number of channels in the experimental decay. Thus, RES reports on the potential of (MC)-FRET to distinguish one scenario from another (for instance, scenario 1 accounting for registered nanodomains from scenario 2 accounting for independent nanodomains). With the help of this parameter, RES diagrams displaying the dependence of the RES parameter on the nanodomain radius $\langle R \rangle$ and surface density $\langle area \rangle$ can be constructed and used to characterize the resolution of MC-FRET as follows: 1) RES $\leq 5\ \%$ (Table 1 and red color code in Figs. 3, 4, 5, 6, 7, and 8), yielding very similar fluorescence decays for scenarios (SCs) 1–4. At the same time, this parameter value corresponds to the relative change in the steady-state intensity of Ds in the presence of As, $\langle F_{DA,SC1} \rangle / \langle F_{DA,SC2} \rangle$, and the intensity-weighted mean fluorescence lifetime, $\langle \tau_{DA,SC1} \rangle / \langle \tau_{DA,SC2} \rangle$, of less than 5% and 4% respectively. Such conditions are unsatisfactory for the characterization of nanodomains by MC-FRET. 2) RES $\in (5; 10\rangle\ \%$ (Table 1 and yellow color code in Figs. 3, 4, 5, 6, 7, and 8), enabling the detection of nanodomains by MC-FRET. This parameter

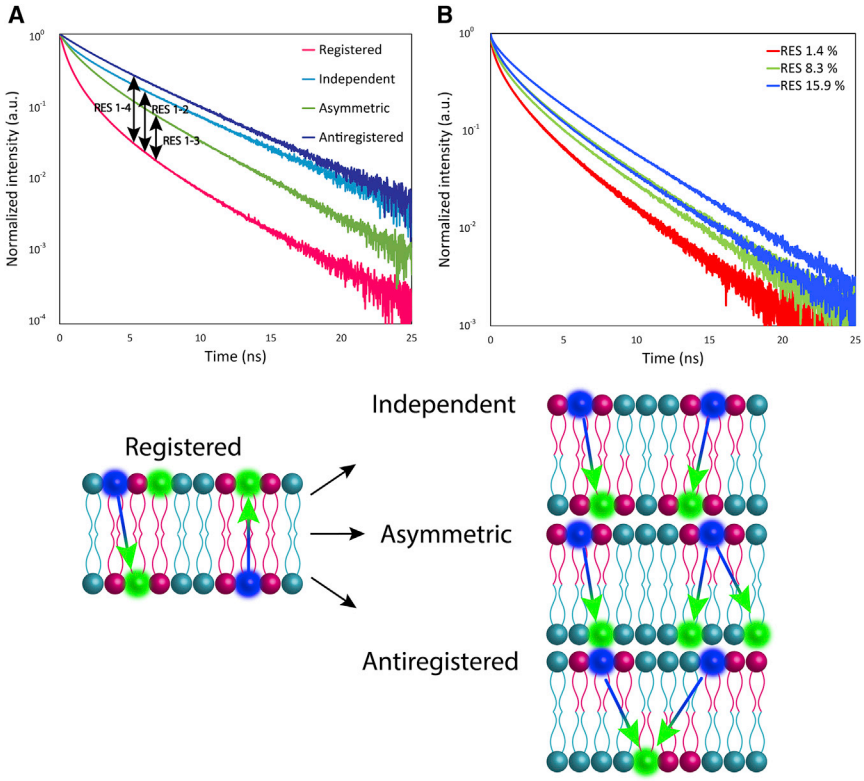

FIGURE 2 The meaning of RES parameter. In the case outlined in (*A*), the parameter expresses the difference between the fluorescence decay generated for the system containing registered nanodomains (*solid magenta curve*) and the systems with either independent (*dotted cyan curve*; yielding the value RES (1-2)), antiregistered (*dashed blue curve*; yielding the value RES (1-3)), or asymmetrically distributed nanodomains (*dash-dotted green curve*; yielding the value RES (1-4)). In (*B*), time-resolved fluorescence decays corresponding to RES = 1.14% (*red decays*), 8.3% (*green decays*), and 15.9% (*blue decays*) are displayed. To see this figure in color, go online.

value is accompanied by $\langle F_{DA,SC1}\rangle/\langle F_{DA,SC2}\rangle \in 5\% - 13\ \%$ and $\langle \tau_{DA,SC1}\rangle/\langle \tau_{DA,SC2}\rangle \in 4\% - 10\ \%$. 3) $RES \in (10;30\rangle\ \%$ (Table 1 and green color code in Figs. 3, 4, 5, 6, 7, and 8), yielding clearly distinct fluorescence decays. This parameter value results in the changes of $\langle F_{DA,SC1}\rangle/\langle F_{DA,SC2}\rangle \in 13\% - 60\ \%$ and $\langle \tau_{DA,SC1}\rangle/\langle \tau_{DA,SC2}\rangle \in 10\% - 30\ \%$. 4) $RES \in (30;60\rangle\ \%$ (Table 1 and cyan color code in Figs. 3, 4, 5, 6, 7, and 8), leading to changes of $\langle F_{DA,SC1}\rangle/\langle F_{DA,SC2}\rangle \in 60\% - 100\ \%$ and $\langle \tau_{DA,SC1}\rangle/\langle \tau_{DA,SC2}\rangle \in 30\% - 50\ \%$. 5) Finally, if $RES > 60\ \%$ (Table 1 and blue color code in Figs. 3, 4, 5, 6, 7, and 8), $\langle F_{DA,SC1}\rangle/\langle F_{DA,SC2}\rangle > 100\ \%$ and $\langle \tau_{DA,SC1}\rangle/\langle \tau_{DA,SC2}\rangle > 50\ \%$.(15)

THE RESOLUTION OF FRET IS CONTROLLED BY PROBES AFFINITY TO NANODOMAINS

The potential of MC-FRET to characterize nanodomain coupling largely depends on which fluorescent probes are chosen as Ds and As of FRET; in particular, it relies on the affinity of D and A to the nanodomains and the region outside of them. In this article, this affinity is expressed in the form of partition coefficients of Ds $K_D(D)$ and As $K_D(A)$ (see methodology for the exact definition). In principle, the following cases can arise. Case 0: $K_D(D) = 1$ and $K_D(A) = 1$. Consequently, D and A are distributed homogenously across the entire bilayer regardless of the presence of nanodomains (Fig. 1 *G*). Such a situation allows for neither the detection of nanodomains nor characterization of their interleaflet arrangement using MC-FRET. Case I: $K_D(D) > 1$ and $K_D(A) > 1$, where both D and A are preferentially localized in nanodomains (Fig. 1 *H*). Case II: $K_D(D) < 1$ and $K_D(A) < 1$, in which both D and A are excluded from nanodomains (Fig. 1 *I*). In this and the previous case, the average distance between D and A is decreased, which results in enhanced FRET and accelerated D relaxation kinetics compared with case 0. And finally, case III: $K_D(D) > 1$ and $K_D(A) < 1$ or $K_D(D) < 1$ and $K_D(A) > 1$, which leads to accumulation of Ds and As in

TABLE 1 RES parameter and its relation to the resolution of FRET, the corresponding relative change in the steady-state intensity and average fluorescence lifetime, and the color code used in RES diagrams.

RES	MC-FRET resolution	Change in the steady-state intensity (%)	Change in the average lifetime (%)	Color in the diagram
$RES \leq 5\%$	unsatisfactory	0–5	0–4	red
$RES \in (5;10\rangle\%$	sufficient	5–13	4–10	yellow
$RES \in (10;30\rangle\%$	satisfactory	13–60	10–30	green
$RES \in (30;60\rangle\%$	good	60–100	30–50	cyan
$RES \geq 60\%$	excellent	>100	>50	blue

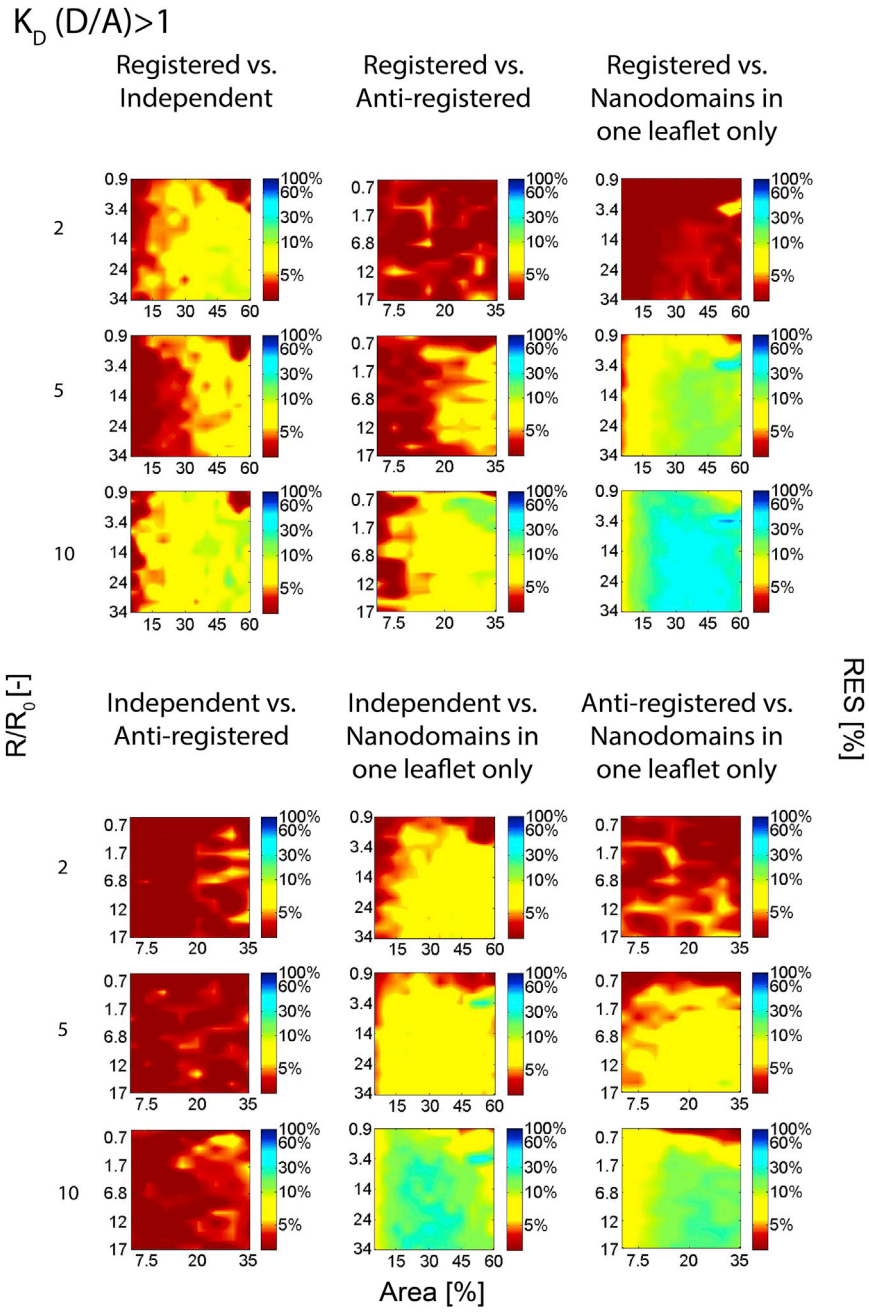

FIGURE 3 Resolution (RES) diagrams displaying the dependence of the RES parameter on the nanodomain radius (R) and relative surface area ($area$) shown for the case when both D and A have increased affinity to the nanodomains ($K_D(D/A) > 1$). To see this figure in color, go online.

distinct bilayer regions and, consequently, spatial separation of Ds from As (Fig. 1 *J*). Such a probe distribution yields a lower efficiency of FRET and slower D relaxation kinetics compared with case 0. In the following text, we are going to discuss cases I-III in more detail.

Case I: Accumulation of D and A in nanodomains ($K_D(D) > 1$ and $K_D(A) > 1$) yields satisfactory resolution

In the simulations, we focused exclusively on the situations where $K_D(D) = K_D(A)$ and generated data for $R/R_0 \in \langle 0.7; 34 \rangle$, which corresponds to the nanodomain radii $R \in \langle 4; 200 \rangle$ nm if a typical value of $R_0 = 58.4$ Å is used and $area \in \langle 5; 60 \rangle$%. If $R/R_0 > 34$, nanodomains can be detected by classical fluorescence microscopy, which eliminates the need of using MC-FRET for nanodomain characterization. Yet, FRET could still be used in the characterization of nanodomain coupling. Moreover, if $area > 60\%$, it becomes sterically impossible to place more nanodomains into the bilayer in such a way that they do not overlap. An exception is represented by antiregistered nanodomains, where it is technically impossible to achieve a density of nanodomains higher than 35% and

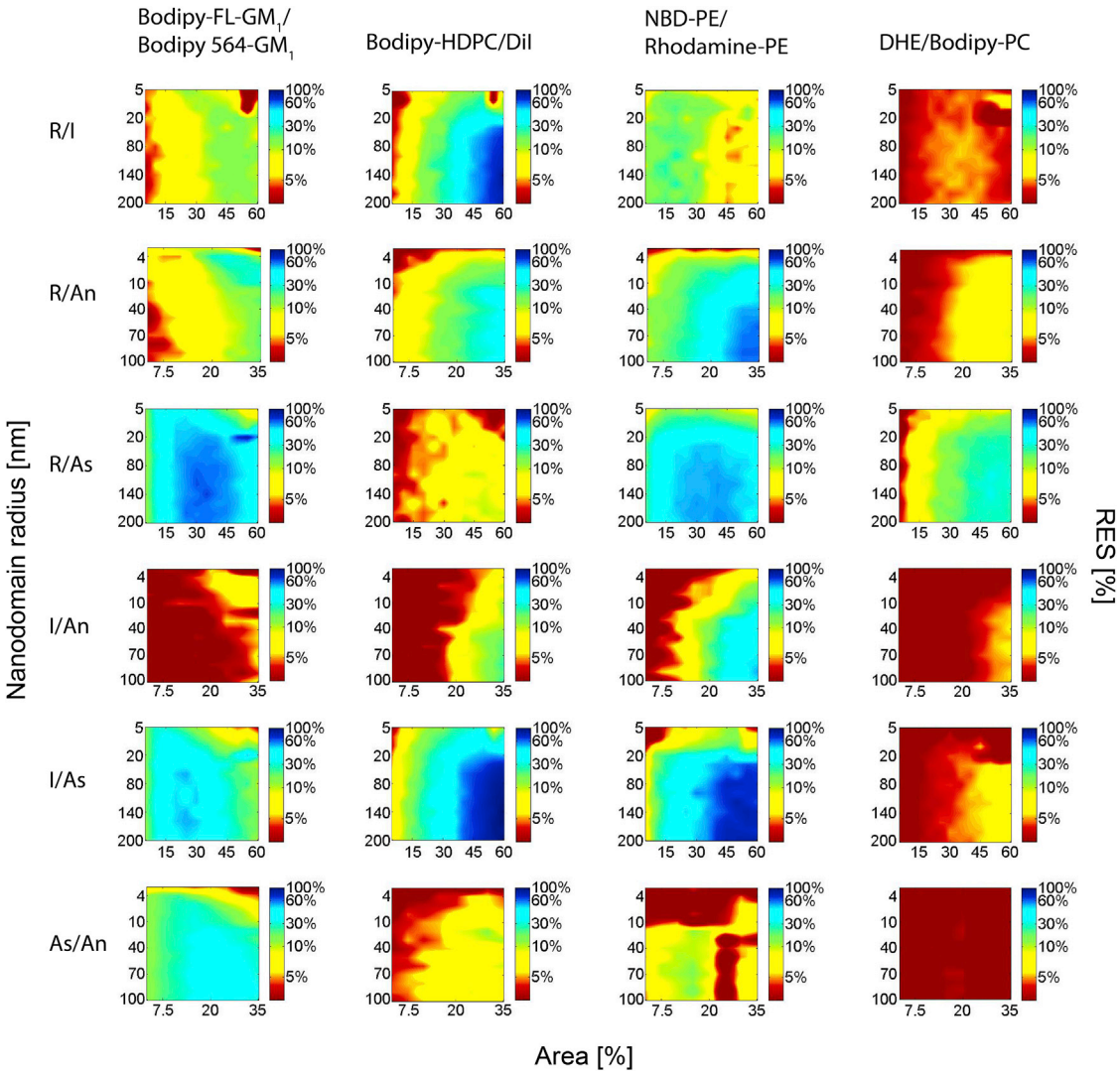

FIGURE 4 RES diagrams calculated for selected D/A pairs (see examples I–IV in the text). D and A chromophores were located at the lipid-water interface. To see this figure in color, go online.

$R/R_0 > 17$. Under these conditions, more nanodomains cannot be generated in the bilayer in a way that nanodomains in both leaflets occupy distinct lateral positions.

As expected, the resolution of FRET is continuously improving as the affinity of D and A to nanodomains increases (Fig. 3). In the main text of this article, we only present the simulations results for $K_D(D, A) \in \langle 2; 10 \rangle$, which covers the range of typical $K_D(D, A)$ values of currently available fluorescent probes (see Table 2 for the list of these probes). As shown in the supporting material, the MC-FRET resolution continues getting better only slightly between $K_D(D, A) \in \langle 10; 100 \rangle$, but beyond $K_D(D, A) > 100$, the resolution is not significantly improved. The continuously improved resolution seems common to all six situations we examined: specifically, the situations where the potential of MC-FRET to resolve registered from independent, registered from antiregistered, or registered nanodomains from the nanodomains localized in one leaflet were investigated (Fig. 3, *top row*). Furthermore, we investigated the capacity of MC-FRET to resolve independent from antiregistered, independent nanodomains from those localized asymmetrically in one leaflet and antiregistered from asymmetrically distributed nanodomains (Fig. 3, *bottom row*).

It is obvious from the RES maps that even for Ds and As having moderate affinity to nanodomains ($K_D(D/A) > 5$), a satisfactory resolution, i.e., a resolution where the red color in the RES diagrams represents a minor component, is achieved for all analyzed situations. The only exception is the SC where independent nanodomains are resolved from antiregistered ones. In this specific case, the nanodomains are distributed over the bilayer surface in a very similar manner, which results in similar time-resolved fluorescence decays, and,

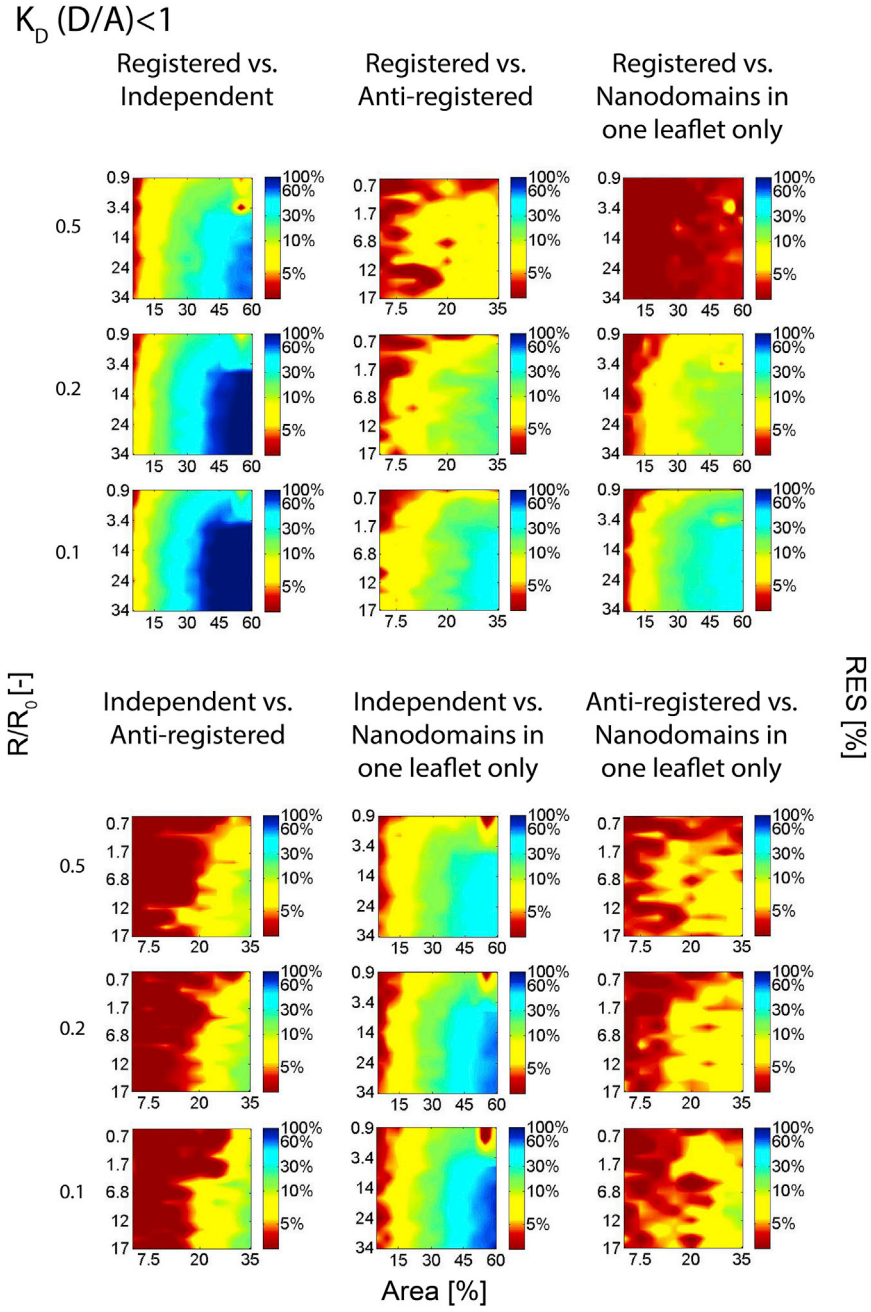

FIGURE 5 RES diagrams shown for the case when both D and A have increased affinity to the regions outside of the nanodomains ($K_D(D/A) < 1$). To see this figure in color, go online.

consequently, poor resolution of MC-FRET. As a rule, it appears most difficult to study nanodomain coupling if they occupy only a small part of the bilayer *area* $\leq$ 10%, independently of the nanodomain size.

Example I: Bodipy-FL-GM$_1$/Bodipy-564/570-GM$_1$ D/A pair ($K_D(D/A) \geq 20, R_0 = 58.4$ Å)

This D/A pair, consisting of fluorescently labeled gangliosides GM$_1$ (Table 3; Fig. 4), exhibits the highest experimentally determined affinity to lipid nanodomains and has already been used in a variety of experimental studies, for instance in the detection and characterization of DOPC/Chol/SM nanodomains, ganglioside nanodomains, or nanodomains containing oxidized phospholipids (8,10,11,13,17,18).

In our recent work, we used this D/A pair to study interleaflet organization of nanodomains by MC-FRET (10). More specifically, we fitted experimentally recorded decays by the models assuming registered, independent, and antiregistered nanodomains and identified the following global minima in the χ^2 space: $\chi^2(\mathrm{REG}) = 1.94$

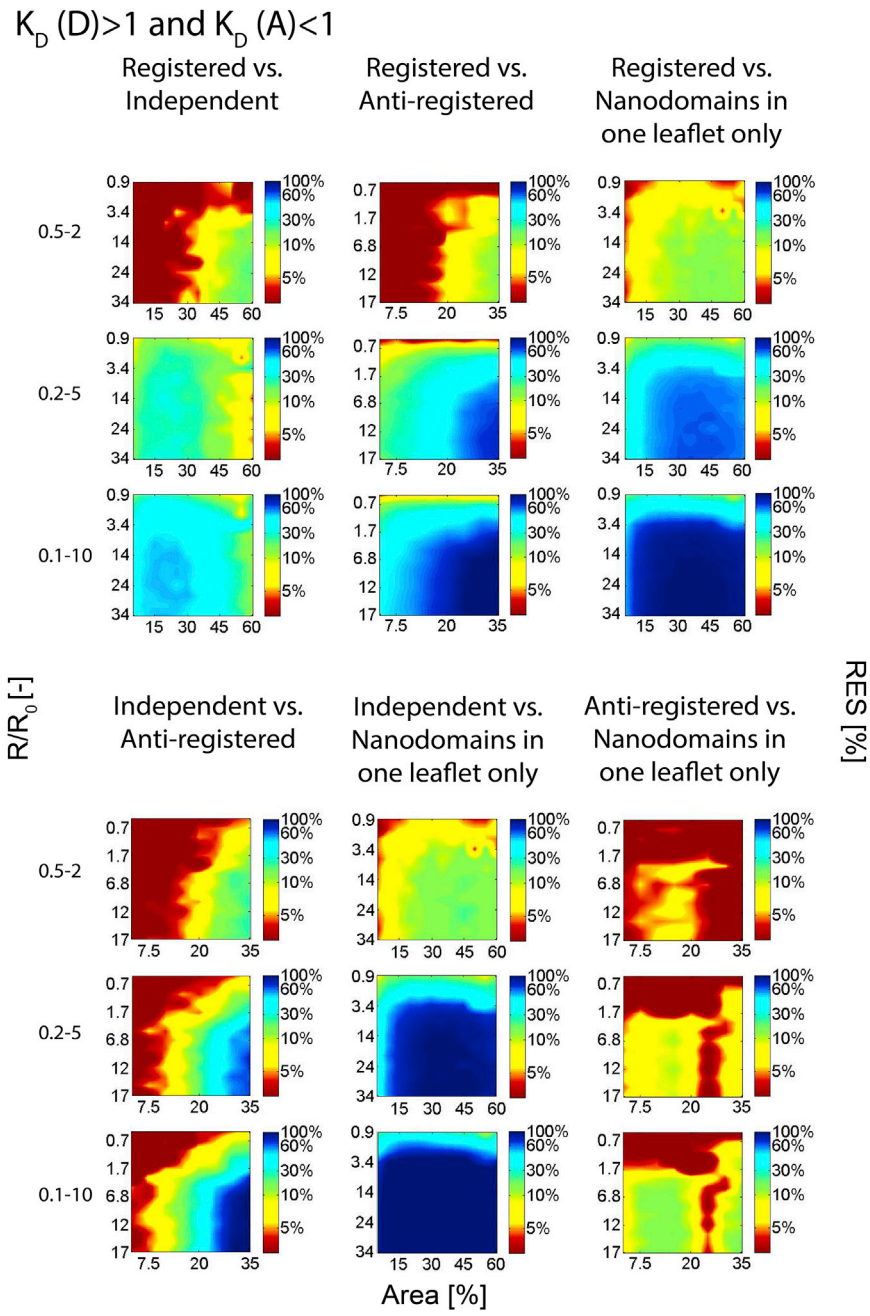

FIGURE 6 RES diagrams shown for the case when Ds have increased affinity to the nanodomains ($K_D(D) > 1$) and As have increased affinity to the regions outside of the nanodomains ($K_D(D/A) < 1$). To see this figure in color, go online.

($R = 78 \pm 17$ nm,*area* $= (63 \pm 5)\%$); $\chi^2(\text{INDEP}) = 4.9$; $\chi^2(\text{ANTIREG}) = 6.76$ (10). In this way, we could show that the nanodomains were registered across the bilayer leaflets.

However, let us stay with this particular case for a while longer. By calculating a ratio between $\chi^2(\text{REG})$ and $\chi^2(\text{INDEP})$, we get a parameter that resembles the above introduced parameter RES, allowing us to characterize the experimental resolution between registered and independent nanodomains. By also calculating the ratio for the remaining two cases, we can compare the results in a more robust way: $\chi^2(\text{REG})/\chi^2(\text{INDEP}) = 2.53$; $\chi^2(\text{REG})/\chi^2(\text{ANTIREG}) = 3.58$; $\chi^2(\text{INDEP})/\chi^2(\text{ANTIREG}) = 1.42$. This comparison shows that registered versus independent or registered versus antiregistered nanodomains can be resolved more safely than independent from antiregistered nanodomains. This experimental result thus fully supports the results of the simulations, which identified the resolution between independent versus antiregistered nanodomains as being the worst (Fig. 3). In other words, the analysis shows a general trend evident for cases I, II, and III, namely that it is easiest to distinguish between registered nanodomains and the other situations or between asymmetrically distributed domains versus the alternative SCs, and what remains as the most

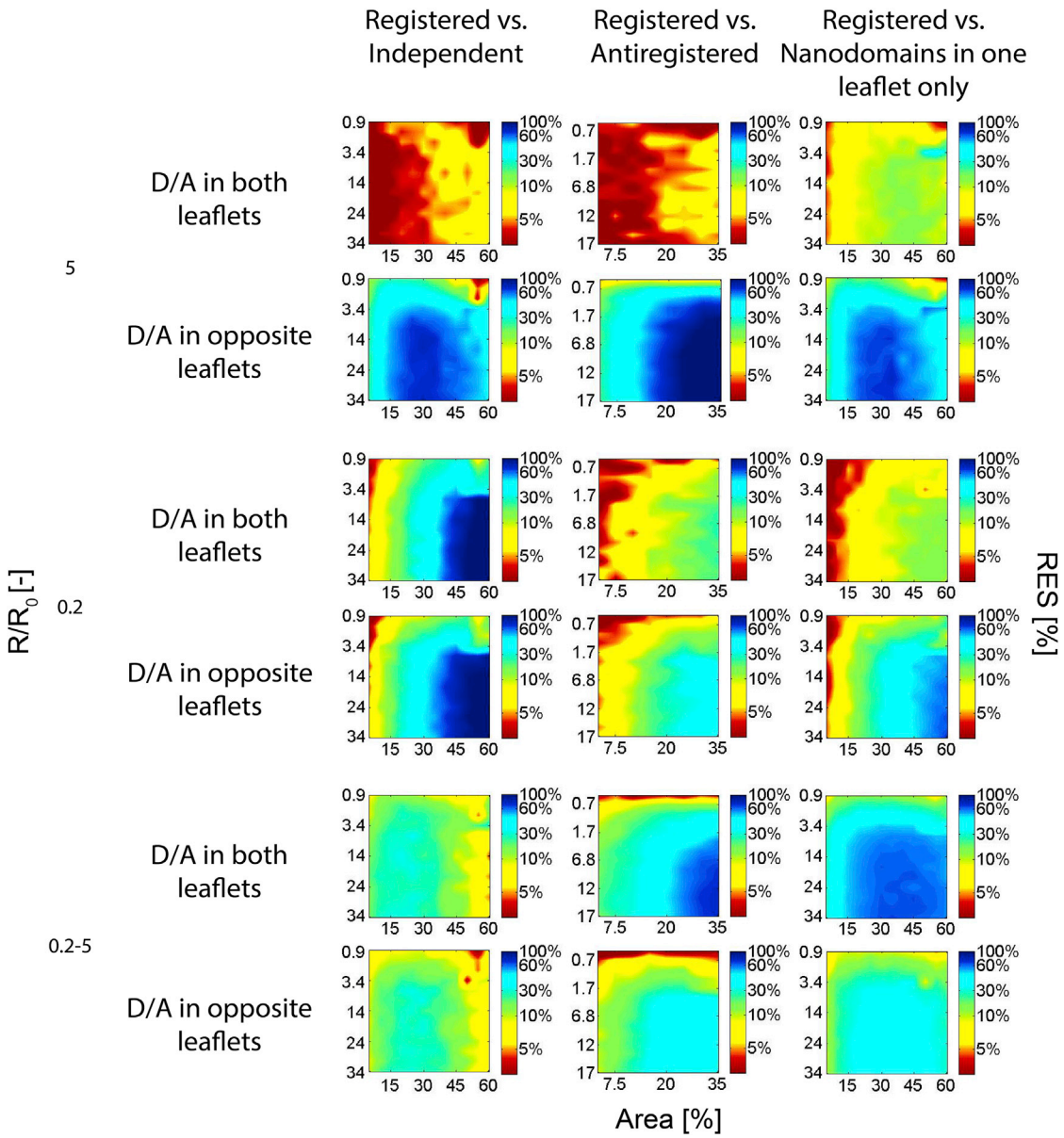

FIGURE 7 RES diagrams demonstrating the improvement of FRET resolution by distributing D and A into opposite bilayer leaflets. The simulations were performed for $K_D(D/A) = 5$; $K_D(D/A) = 0.2$; and $K_D(D) = 5$ & $K_D(A) = 0.2$. In this figure, the resolution between registered nanodomains and independent/antiregistered/asymmetrically distributed nanodomains has been investigated. To see this figure in color, go online.

challenging to distinguish is independent from antiregistered nanodomains.

Case II: Accumulation of D and A in the nondomain region ($K_D(D) < 1$ and $K_D(A) < 1$) yields improved resolution

Since fluorescent probes that would be localized exclusively in one of the regions do not practically exist ($K_D(D/A) \ll 1$), we constrain our discussion here to the ones having $K_D(D,A) \in \langle 0.1; 1\rangle$. At the same time, we show more results for $K_D(D,A) \in \langle 0.01; 1\rangle$ in the supporting material. For an efficient comparison of cases I, II, and III, it should also be noted that D and A having $K_D(D/A) = X$ or $K_D(D/A) = 1/X$, where X is an arbitrary number, show the same affinity to the nanodomains or the regions outside of them.

Case II provides somewhat better resolution between registered and independent nanodomains compared with the remaining five situations. And, as in case I, it appears, experimentally, the most challenging to resolve antiregistered from independent nanodomains and, in this case, also antiregistered nanodomains from nanodomains localized in one leaflet only (Fig. 5). Generally, case II appears more advantageous for the characterization of nanodomain coupling than the case I (compare Figs. 3 and 5 using the

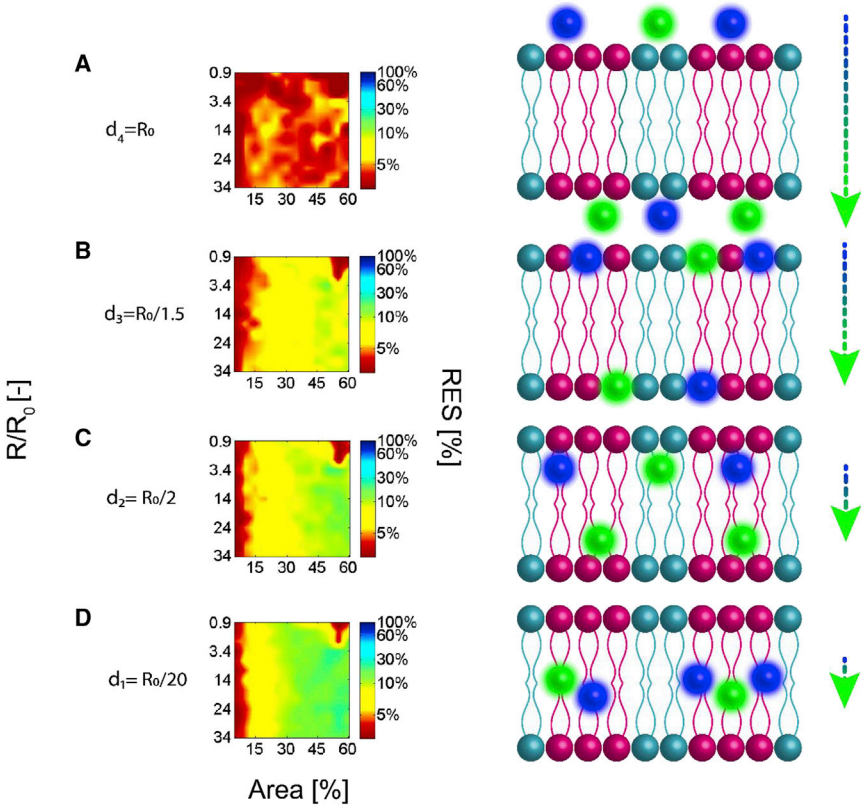

FIGURE 8 The impact of the of the interlayer distance d on the resolution of MC-FRET. Chromophores (donors, *blue*; acceptors, *green*) with $K_D(D/A) = 10$ were assumed to be localized along the bilayer normal in the following ways: 1) fully exposed to the bulk with the interlayer distance $d = R_0$; 2) localized close to the lipid-water interface ($d = R_0/1.5$); 3) localized below the lipid-water interface ($d = R_0/2$); or 4) deeply buried in the membrane close to the bilayer center ($d = R_0/20$). D and A were assumed to be localized in both bilayer leaflets; $R_0 = 58.7$ Å (Table 3). To see this figure in color, go online.

same value of X). The RES maps exhibit a strong "capital lambda" shape, indicating that the lower resolution is achieved for the nanodomains with $R/R_0 < 3.4$ and $area < 15\%$ (Fig. 5). Although not so clearly, this characteristic shape is also evident for case I (Fig. 3). Overall, a satisfactory resolution is reached for all the situations as early as for $K_D(D/A) = 0.2$, thereby significantly expanding the selection of suitable Ds and As that can be used for the analysis (see (15) or Table 2 for the most up-to-date list of suitable fluorescent probes).

Example II: Bodipy-HDPC/fast DiI D/A pair ($K_D(D/A) = 0.1, R_0 = 65$ Å)

This D/A pair consisting of 1-hexadecanoyl-sn-glycero-3-phosphocholine labeled by Bodipy (D) and DiI (A) (Table 3; Fig. 4) is characterized by the highest reported affinity for the nondomain region (Table 2) and large R_0, therefore guarantying the best resolution that can be reached nowadays when using "nondomain probes." The pair has been used to characterize the phase behavior of GUVs (22,25) and belongs to popular D/A pairs in cell biology (26). Overall, this D/A pair exhibits good resolution characteristics that are comparable to the Bodipy-FL-GM_1/Bodipy-564/570-GM_1 D/A pair. More specifically, this and similar D/A pairs are suitable to resolve registered or asymmetrically distributed nanodomains from the alternative situations. Regarding the last "problematic" SC, where independent nanodomains are being resolved from antiregistered ones, nanodomain coupling is under the detection limit only if nanodomains occupy less than 20% of the membrane. Additionally, it becomes experimentally challenging to resolve antiregistered versus asymmetrically distributed nanodomains if they are smaller than 40 nm and occupy less than 10% of the membrane (Fig. 4).

Case III: Accumulation of D and A in distinct bilayer regions ($K_D(D) > 1$ and $K_D(A) < 1$) yields the most robust resolution

In this case, high RES values are characteristic for all investigated situations (Fig. 6) when using probes with a reasonably high affinity to the (non)domain region ($K_D(D) > 5$ and $K_D(A) < 0.2$). Specifically, RES reaches significantly higher values than for case I and case II (using the same value of X for this comparison) and remains high enough even for small nanodomains covering a low fraction of the membrane (compare Figs. 3 and 5 with 6). Although it remains the most difficult to distinguish independent form antiregistered or antiregistered nanodomains from those localized asymmetrically in one leaflet, as in cases I and II, the resolution is perfectly adequate. Overall, considering that case III provides good RES for all the situations for $K_D(D) > 5$ and $K_D(A) < 0.2$, it appears as the most robust case that should be used to guarantee stable high RES for all SCs that can arise (Fig. 1, *A–D*).

TABLE 2 The list of fluorescent probes with either increased or decreased affinity to lipid domains.

	Fluorophore	KD	Lipid composition	Ref.
Probes with affinity to the nondomain region	NBD-DLPE[a]	0.21/0.41	DLPC/DSPC[b] (60:40/40:60)	(19)
	DiIC18(3)	0.15/0.15	DLPC/DSPC[b] (60:40/40:60)	
	BODIPY-PC (16:0)	0.16 ± 0.025	bSM[c]/DOPC/POPC/Chol (40/40/20)	(20)
	rhodamine-DOPE	0.37 ± 0.06	PSM[d]/POPC/Chol (33/33/33)	(21)
	BODIPY-HDPC[e]	0.1	DOPC/DSPC[b]/Chol (35/35/30)	(22)
	fast-DiI	0.1	DOPC/DSPC[b]/Chol (35/35/30)	
	DiD	0.004 ± 0.002	DOPC/SM/Chol/DOPG/GM1 (23–68/0-45/25/5/2)	(23)
	TOE[f]	0.1 ± 0.01	bSM[c]/DOPC/POPC/Chol (40/40/20)	(20)
Probes with affinity to domain region	Bodipy FL-GM1	10	DOPC/SM (85–90/10-15)	(8)
	Bodipy 564/570-GM1	10	DOPC/SM (85–90/10-15)	
	Bodipy FL-GM1	≥20	DOPC/Chol/SM (65–70/25/5–10)	
	Bodipy 564/570-GM1	≥20	DOPC/Chol/SM (65–70/25/5–10)	
	Alexa 488-CTxB[g]	6 ± 3	DOPC/SM/Chol/DOPG/GM1 (23–68/0-45/25/5/2)	(23)
	NBD-DPPE	4.3 ± 1.2	PSM[d]/POPC/Chol (33/33/33)	(21)
	DHE	3.7	bSM[c]/DOPC/POPC/Chol (40/40/20)	(20)
	NBD-DHPE	2.2	DPhPC[h]/DPPC/Chol (40/35/25)	(24)

Note that the KD values reported in this table are strictly related to the listed lipid compositions, and their values must be determined again for other lipid compositions.
[a]N-(7-nitrobenz-2-oxa-1,3-diazol-4-yl)-dilauroylphosphatidylethanolamine.
[b]Distearoylphosphatidylcholine.
[c]Sphingomyelin - brain.
[d]Palmitoyl sphingomyelin.
[e]2-(4,4-difluoro-5,7-dimethyl-4-bora-3a,4a-diaza-s-indacene-3-pentanoyl)-1-hexadecanoyl-sn-glycero-3-phosphocholine.
[f]Tryptophan oleoyl ester.
[g]Alexa Fluor 488-cholera toxin.
[h]Diphytanoylphosphatidyl choline.

Example III: NBD-DPPE/rhodamine-DOPE ($K_D(D) = 4.3$ and $K_D(A) = 0.37, R_0 = 64.1$ A)

This popular NBD-PE/Rh-PE FRET pair has been predominantly used in a vast majority of lipid mixing experiments in membrane fusion studies (27,28). Importantly, DPPE and DOPE lipids conjugated with NBD and rhodamine, respectively, have also been used in a pioneering study by de Almeida et al., in which the authors discovered lipid nanodomains in artificial membranes (21). Although the study did not give any accurate estimate regarding the nanodomain size, relative surface area occupied by nanodomains, or interleaflet organization of nanodomains, the study represents, to our best knowledge, the first experimental study where FRET was used to detect membrane nanodomains.

As shown in Fig. 4, this D/A pair would show excellent results in the studies of nanodomain organization, even though the affinity of this pair to the (non)domain region does not reach the maximum values that have been reported so far (compare the values on Table 2). More specifically, all coupling SCs can be resolved from each other, with the exception of less likely situations when distinguishing independent versus antiregistered nanodomains if $area < 10\%$ or when distinguishing antiregistered versus asymmetrically distributed nanodomains if $R < 9$ nm.

Switching off intra-FRET: Does it lead to improved resolution?

In lipid bilayers, FRET occurs not only within one bilayer leaflet (intra-FRET) but also from one leaflet to the other one (inter-FRET) (10,18,29). Both processes take place simultaneously and independently of each other (Fig. 1). However, since only inter-FRET can uncover how nanodomains are organized between opposite bilayer leaflets, we were interested in whether the resolution could not be further improved

TABLE 3 The main properties (including the probe affinity to the (non)domain region and the Förster radius R0) of the D/A pairs presented in examples I–IV.

D	A	KD(D)	KD(A)	Lipid composition	R0 (nm)	Ref
DHE	Bodipy-PC (16:0)	3.7	0.16 ± 0.025	bSM/DOPC/POPC/Chol (40/40/20)	2.8	(20)
Bodipy FL -GM1	Bodipy 564 -GM1	≥20	≥20	DOPC/Chol/SM (65–70/25/5–10)	5.87	(8)
NBD-DPPE	Rhodamine-DOPE	4.3 ± 1.2	0.37 ± 0.06	PSM/POPC/Chol (33/33/33)	6.41	(21)
BODIPY-HDPC	Fast DiI	0.1	0.1	DOPC/DSPC/Chol (35/35/30)	6.5	(22)

Note that the K_D values reported in this table are strictly related to the listed lipid compositions, and their values must be determined again for other lipid compositions.

by eliminating the possibility of intra-FRET. In the simulations, we, therefore, decided to switch off intra-FRET by placing D in one layer and A in the other layer and to investigate whether this will lead to improved resolution of MC-FRET. Thanks to recent experimental advances, a setup where D and A are located in opposite layers represents not only a hypothetical SC but also a real experimental possibility. As shown in Doktorova et al. (30), asymmetric lipid bilayers, i.e., bilayers consisting of leaflets with different lipid compositions, can be prepared by intervesicular exchange of outer leaflet lipids catalyzed by methyl-β-cyclodextrin. In this way, D in the outer leaflet could be replaced by A contained in exchange vesicles.

For better comparison, the results of simulations are presented in Fig. 7 where cases I, II, and III are represented by $K_D(D/A) = 5$; $K_D(D/A) = 0.2$; $K_D(D) = 5$ and $K_D(A) = 0.2$, respectively. Indeed, the resolution improves but only for case I, where a satisfactory resolution is reached for $K_D(D/A)$ as low as 2, and only slightly for case II. In contrast, the RES remains constant or even gets a little worse for case III. The degree of improvement is primarily determined by the extent to which intra-FRET is competitive for inter-FRET: the improvement is the most prominent for case I, where intra-FRET is extraordinarily efficient due to the entrapment of D and A within the nanodomains and is insignificant for case III, where D and A are separated from each other even when they are distributed symmetrically in both leaflets. Thus, by locating D and A into opposite leaflets, only the resolution for case I is improved, and it reaches similar results as the most robust case III with the probes equally distributed between the leaflets.

D/A pairs with a short Förster radius do not provide sufficient resolution

Finally, since it is widely known that the efficiency of FRET decreases quickly with the distance between a D and an A, we set out to investigate the resolution of FRET as a function of the interlayer distance d. This distance, defined as the distance at which D and A in one leaflet are transversally separated from D and A in the other leaflet (Fig. 8), controls the efficiency of inter-FRET that is responsible for the sensitivity of FRET to the organization of nanodomains.

We simulated FRET for four different interlayer distances: $d \in \{R_0; R_0/1.5; R_0/2; R_0/20\}$. By assuming a typical value of $R_0 = 58.7$ Å (see Table 3), D and A would be 1) fully exposed to the bulk ($d = R_0$); 2) localized close to the lipid-water interface ($d = R_0/1.5$); 3) localized below the lipid-water interface ($d = R_0/2$); or 4) deeply buried in the membrane close to the bilayer center ($d = R_0/20$) (Fig. 8). In this case, D and A basically occupy the same plane that is located at the bilayer center (Fig. 8 *D*).

The analysis of Fig. 8 shows that the best resolution is obtained when D and A are located in the bilayer center. Although the resolution is declining slowly in the range $d \in [R_0/20; R_0]$, any D/A pair whose R_0 exceeds the bilayer thickness is perfectly suitable for the characterization of nanodomain coupling. As shown in the following example, since the resolution deteriorates rapidly for $d > R_0$, care should be taken when selecting probes with a short R_0.

Example IV: DHE/Bodipy-PC(16:0) ($K_D(D) = 3.7$ and $K_D(A) = 0.16, R_0 = 28$ **A)**

This D/A pair exhibits a reasonable affinity for the (non) domain region and thus represents a good D/A pair for the detection of nanodomains and the determination of their size (13). At the same time, however, this pair has a short Förster radius, which reduces its sensitivity to the interleaflet organization of nanodomains (Fig. 4). The final resolution depends on the vertical positions of DHE and Bodipy chromophores. Whereas the chromophore of Bodipy-PC is located close to the lipid-water interface (like the chromophores selected for examples I–III) (16), the location of DHE is less clear. Nevertheless, under the extreme assumptions that DHE is located either at the lipid-water interface or close to the bilayer center, the resolution appears poor in both cases (only the case when DHE is located at the interface is shown in Fig. 4). This D/A pair is thus suitable only for the detection of nanodomains but less suitable for the research of nanodomain coupling.

Design of an MC-FRET experiment and the applicability of the approach

Knowing the possibilities and limits of FRET, the next logical step is to use MC-FRET to determine the size, concentration, and interleaflet organization of nanodomains in real lipid membranes. Up to now, the method has been used in the membranes of GUVs (8,17,23,31,32), as well as large unilamellar vesicles (31) and recently also in the membranes of giant plasma membrane vesicles (GPMVs) (7). In this last specific case, however, the study did not focus on the characterization of membrane nanodomains but rather the quantification of protein dimerization in the membrane using the same MC-FRET methodology. Overall, success depends on determining as many parameters as possible that enter the simulation in an independent way. For clarity, we have summarized the most important parameters in Table 4, and as the following text implies, most of the parameters can be determined independently before starting the optimization procedure. The parameters including the Förster radius, the decay of Ds in the absence of As, and the width of the lipid bilayer but also the transversal localization of D and A chromophores within the lipid bilayer (16) (Table 4) can be determined/measured straightforwardly and input into the simulation prior to its start. In our research, we have used Bodipy-based chromophores, which are located universally close to the lipid/water interface (8,16,17). Thus, the parameters that remain to be

TABLE 4 Input parameters entering the MC-FRET simulation

Parameter	Abbreviation	Value	
Förster radius	R_0	58.7 Å[a]	
Interlayer distance	D	37.5 Å[b]	
Coupling scenarios	–	registered/independent/ antiregistered/asymmetric	
Average nanodomain radius	$\langle R \rangle$	antiregistered domains	others
		4–100 nm	5–200 nm
Relative surface area occupied by nanodomains (%)	$\langle area \rangle$	5%–35%	5%–60%
Surface concentration of D/A	c(D/A)	0.5%/0.5%[b]	
Partition coefficient of D/A	K_D(D/A)	0.1–10	

[a]A value determined for Bodipy-FL (D) and Bodipy-564/570 (A).
[b]If not stated differently.

determined comprise the surface concentration of Ds, c(D), and As, c(A), in the membrane, the K_D(D) and K_D(A), the nanodomain radius $\langle R \rangle$, the surface density of nanodomains $\langle area \rangle$, and, finally, the interleaflet organization of nanodomains.

As shown recently by Škerle et al. (7), the concentrations c(D) and c(A) in the membranes of GPMVs or GUVs can be determined, for instance, by z-scan fluorescence correlation spectroscopy by constructing a calibration curve that relates the intensity of D and A located in the membrane with the corresponding concentration. Alternatively, we developed an approach applicable to large unilamellar vesicles, GUVs, and GPMVs that is based on the determination of c(D) and c(A) by FRET (15,33). This approach builds upon the so-called Bauman-Fayer model, which provides the surface concentration (34) as one of the fitting parameters for homogeneous vesicles that have a composition as close as possible to that of nanoscopically heterogeneous membranes.

The robustness of the method will further increase if K_D(D) and K_D(A) can also be determined independently for the particular mixture of interest. This is, however, not always possible, but, very often, an MC-FRET experiment can be designed in such a way that the range of possible K_D values is noticeably limited, e.g., when studying ganglioside nanodomains or nanodomains enriched by sphingomyelin, headgroup-labeled gangliosides with exclusive localization in lipid domains ($K_D(D/A) \geq 10$) have proved useful. From the analyses carried out at that time, it emerged that the position of the global minima did not change over a wide range of $K_D(D/A) \geq 5$. In a similar study, we determined the size and concentration of cholera toxin nanodomains using Alexa-488-labeled cholera toxin (D, as expected, localized in the domains) and DiD As excluded from those nanodomains with significantly ordered character (31). In an optimistic real-world scenario, the number of optimized parameters can thus be reduced to only three: the nanodomain radius $\langle R \rangle$, the surface density of nanodomains $\langle area \rangle$, and the interleaflet organization of nanodomains. In our fitting routine, we first scan the chi-squared space by sequentially changing $\langle R \rangle$ and $\langle area \rangle$ for a given organization of nanodomains and then repeat the same procedure for the alternative coupling SCs. In this way, we obtain a three-dimensional matrix of chi-squared values, in which we search for global and possibly other secondary minima. This procedure guarantees that we do not overlook similarly deep minima. For instance, in the lipid mixture consisting of DOPC/SM (90/10), we found two equally deep minima centered at $\langle R \rangle = 8$ nm and $\langle area \rangle = 37\%$ and at $\langle R \rangle = 12$ nm and $\langle area \rangle = 55\%$ (8) without knowing which of these minima corresponded to reality. In a less optimistic situation when the final K_D values are not known at all, it is still possible to repeat the entire fitting procedure for a set of different K_Ds and try to localize the global minima corresponding to the real values of the unknown parameters.

Purely out of our curiosity, we also carried out a completely different analysis as part of this work, described in detail in the supporting material. Briefly, we generated time-resolved fluorescence decays corresponding to the settings specified in Table S1. In the rest of the analysis, we treated these decays as experimentally recorded decays. We, therefore, fitted these decays using models considering registered, independent, antiregistered, or asymmetrically distributed nanodomains (SCs 1–4). In the final step, we compared the obtained chi-squared values characterizing the quality of the fit as well as the input and output parameters of the simulation: $\langle R \rangle$, $\langle area \rangle$, and possibly $K_D(D/A)$. This analysis ultimately shows that FRET does have the potential to characterize nanodomain coupling, as concluded in the article. However, caution is warranted if there is no information on possible $K_D(D/A)$ values. In such a case, it cannot be ruled out that the analysis will provide several global minima as the final output, and it is then only up to the experimentalist to further narrow down the set of possible local minima.

The situation is noticeably more complicated in plasma membranes of living cells, in which the number of unknown parameters cannot be constrained as effectively as in the membranes of lipid vesicles. The local concentrations of D and A may vary, for instance, due to local membrane curvature or local inhomogeneities, and it is generally more difficult to make any qualified estimate about the values of K_Ds. Consequently, one may be less lucky in obtaining reliable information about the coupling of nanodomains. But it is true that this approach will first need to be tested experimentally to find its limits when applied to cellular membranes. Of note, a reasonable compromise on the way from model to cellular membranes may consist of GPMVs. These vesicles have a flat membrane, and, as shown in Skerle et al. (7), the list of unknown parameters that enter the simulation may be shortened considerably.

CONCLUSIONS: CRITICAL PARAMETERS THAT CONTROL THE RESOLUTION AND SUITABLE D/A PAIRS

The analysis presented in this article identified the following experimental parameters as the most critical in the characterization of nanodomain coupling.

First, the Förster radius and its value related to the interlayer distance d, at which D and A in one leaflet are transversally separated from D and A in the other leaflet (Fig. 8). Depending on this parameter, the resolution appears relatively stable in the range $d \in [R_0/20; R_0/1.5]$: it is the best when D and A are located in the bilayer center, i.e., if $d \ll R_0$ (see Fig. 8), and declines sharply beyond this range. Since most fluorescent probes used nowadays are located at the lipid-water interface, R_0 should not be lower than the bilayer thickness.

Second, the resolution of FRET is controlled by the affinity of D and A to the (non)domain region. Although the affinity of available probes is generally low (Table 2), the K_Ds are high/low enough to allow for characterization of nanodomain organization with unprecedented detail. More specifically, D and A having moderate affinity to the nanodomains ($K_D(D/A) > 5$) or the nondomain region ($K_D(D/A) < 0.2$) can resolve registered from independent, antiregistered, or asymmetrically organized nanodomains as well as asymmetrically distributed nanodomains from independent or antiregistered ones in a broad range of nanodomain radii $R/R_0 \geq 2$ and relative surface area occupied by the nanodomains $area \geq 10\%$ (compare Figs. 3, 5, and 6). At the same time, it appears experimentally challenging to distinguish independent from antiregistered nanodomains since, in this case, nanodomains are distributed over the bilayer surface in a very similar manner. Of all three cases (I, II, and III) analyzed, case III, where D and A exhibit opposite, reasonably high affinity to the nanodomains and the region outside of them ($K_D(D) > 5$ and $K_D(A) < 0.2$), provides the best resolution.

Third, the resolution of the method depends on the extent to which inter-FRET is competitive with intra-FRET, and, as expected, the method performs worst if intra-FRET is dominant. This is most evident in case I ($K_D(D) > 1$ and $K_D(A) > 1$), where D and A are located in the nanodomains. In this case, however, the RES can be improved by placing D and A into opposite bilayer leaflets, thereby eliminating intra-FRET.

According to our analysis, the best performance offer Bodipy-FL-GM_1/Bodipy-564/570-GM_1 ($K_D(D/A) \geq 20, R_0 = 58.4$ Å) or NBD-DPPE/rhodamine-DOPE ($K_D(D) = 4.3$ and $K_D(A) = 0.37$, $R_0 = 64.1$ Å) D/A pairs. Both D/A pairs reach a satisfactory RES except in extreme conditions when nanodomains are small (nanodomain radius <10 nm or $R/R_0 = 3.4$) or occupy a small part of the lipid bilayer (surface density of nanodomains <10%). Overall, MC-FRET appears as a robust method that, when using D/A pairs with good characteristics, yields otherwise difficult-to-reach characteristics of membrane lipid nanodomains.

SUPPORTING MATERIAL

Supporting material can be found online at https://doi.org/10.1016/j.bpj.2022.11.014.

AUTHOR CONTRIBUTIONS

R.Š. conceived the idea; B.C. and R.Š. developed the simulation code; B.C. performed the simulations and analyzed the data with help of D.D.; B.C. and R.Š. interpreted the data and wrote the manuscript; and all authors revised the manuscript.

ACKNOWLEDGMENTS

R.Š., B.C., and D.D. acknowledge GAČR grant 20-01401J. R.Š. acknowledges the European Commission Horizon 2020 research and innovation program under grant agreement no. 101017902. B.C. would like to acknowledge project no. SVV 260586 of Charles University. Computational resources were supplied by the project "e-Infrastruktura CZ" (e-INFRA CZ LM2018140) supported by the Ministry of Education, Youth and Sports of the Czech Republic. We thank Prof. Martin Hof for reading the manuscript and providing useful comments.

DECLARATION OF INTERESTS

The authors declare no competing interests.

REFERENCES

1. Nickels, J. D., J. C. Smith, and X. Cheng. 2015. Lateral organization, bilayer asymmetry, and inter-leaflet coupling of biological membranes. *Chem. Phys. Lipids.* 192:87–99.
2. Grzybek, M., T. Gutmann, and Ü. Coskun. 2014. Cell Membrane Nanodomains. CRC Press.
3. Goñi, F. M., A. Alonso, and F. X. Contreras. 2020. Membrane nanodomains. *In* eLS Wiley, pp. 1–8.
4. Bernardino de la Serna, J., G. J. Schütz, …, M. Cebecauer. 2016. There is No simple model of the plasma membrane organization. *Front. Cell Dev. Biol.* 4:106–117.
5. Cebecauer, M., M. Amaro, …, M. Hof. 2018. Membrane lipid nanodomains. *Chem. Rev.* 118:11259–11297.
6. Owen, D. M., A. Magenau, …, K. Gaus. 2012. The lipid raft hypothesis revisited - new insights on raft composition and function from super-resolution fluorescence microscopy. *Bioessays.* 34:739–747.
7. Škerle, J., J. Humpolíčková, …, K. Strisovsky. 2020. Membrane protein dimerization in cell-derived lipid membranes measured by FRET with MC simulations. *Biophys. J.* 118:1861–1875.
8. Koukalová, A., M. Amaro, …, R. Šachl. 2017. Lipid driven nanodomains in giant lipid vesicles are fluid and disordered. *Sci. Rep.* 7:5460.
9. Ashrafzadeh, P., and I. Parmryd. 2015. Methods applicable to membrane nanodomain studies? *Essays Biochem.* 57:57–68.
10. Vinklárek, I. S., L. Vel'As, …, R. Šachl. 2019. Experimental evidence of the existence of interleaflet coupled nanodomains: an MC-FRET study. *J. Phys. Chem. Lett.* 10:2024–2030.

11. Sarmento, M. J., M. Hof, and R. Šachl. 2020. Interleaflet coupling of lipid nanodomains – insights from in vitro systems. *Front. Cell Dev. Biol.* 8:284.
12. Blosser, M. C., A. R. Honerkamp-Smith, …, S. L. Keller. 2015. Transbilayer colocalization of lipid domains explained via measurement of strong coupling parameters. *Biophys. J.* 109:2317–2327.
13. Šachl, R., J. Humpolíčková, …, M. Hof. 2011. Limitations of electronic energy transfer in the determination of lipid nanodomain sizes. *Biophys. J.* 101:L60–L62.
14. King, C., V. Raicu, and K. Hristova. 2017. Understanding the FRET signatures of interacting membrane proteins. *J. Biol. Chem.* 292: 5291–5310.
15. Chmelová, B., J. Humpolíčková, …, R. Šachl. 2022. The analysis of in-membrane nanoscopic aggregation of lipids and proteins by MC-FRET. *In* Fluorescence Microscopy and Spectroscopy in Biology. R. Šachl and M. Amaro, eds Springer, in press.
16. Šachl, R., I. Boldyrev, and L. B. A. Johansson. 2010. Localisation of BODIPY-labelled phosphatidylcholines in lipid bilayers. *Phys. Chem. Chem. Phys.* 12:6027–6034.
17. Sarmento, M. J., M. C. Owen, …, R. Šachl. 2021. The impact of the glycan headgroup on the nanoscopic segregation of gangliosides. *Biophys. J.* 120:5530–5543.
18. Sarmento, M. J., J. C. Ricardo, …, R. Šachl. 2020. Organization of gangliosides into membrane nanodomains. *FEBS Lett.* 594:3668–3697.
19. Loura, L. M., A. Fedorov, and M. Prieto. 2000. Partition of membrane probes in a gel/fluid two-component lipid system: a fluorescence resonance energy transfer study. *Biochim. Biophys. Acta Biomembr.* 1467:101–112.
20. Enoki, T. A., F. A. Heberle, and G. W. Feigenson. 2018. FRET detects the size of nanodomains for coexisting liquid-disordered and liquid-ordered phases. *Biophys. J.* 114:1921–1935.
21. De Almeida, R. F. M., L. M. S. Loura, …, M. Prieto. 2005. Lipid rafts have different sizes depending on membrane composition: a time-resolved fluorescence resonance energy transfer study. *J. Mol. Biol.* 346:1109–1120.
22. Heberle, F. A., J. Wu, …, G. W. Feigenson. 2010. Comparison of three ternary lipid bilayer mixtures: FRET and ESR reveal nanodomains. *Biophys. J.* 99:3309–3318.
23. Štefl, M., R. Šachl, …, M. Hof. 2012. Dynamics and size of cross-linking-induced lipid nanodomains in model membranes. *Biophys. J.* 102:2104–2113.
24. Bordovsky, S. S., C. S. Wong, …, D. Y. Sasaki. 2016. Engineering lipid structure for recognition of the liquid ordered membrane phase. *Langmuir.* 32:12527–12533.
25. Taylor, G. J., F. A. Heberle, …, S. A. Sarles. 2017. Capacitive detection of low-enthalpy, higher-order phase transitions in synthetic and natural composition lipid membranes. *Langmuir.* 33:10016–10026.
26. Okuno, D., R. Iino, and H. Noji. 2013. Encyclopedia of Biophysics. Springer Berlin Heidelberg, Berlin, Heidelberg.
27. Struck, D. K., D. Hoekstra, and R. E. Pagano. 1981. Use of resonance energy transfer to monitor membrane fusion. *Biochemistry.* 20: 4093–4099.
28. Lira, R. B., T. Robinson, …, K. A. Riske. 2019. Highly efficient protein-free membrane fusion: a giant vesicle study. *Biophys. J.* 116:79–91.
29. Franzl, T., D. S. Koktysh, …, N. Gaponik. 2004. Fast energy transfer in layer-by-layer assembled CdTe nanocrystal bilayers. *Appl. Phys. Lett.* 84:2904–2906.
30. Doktorova, M., F. A. Heberle, …, D. Marquardt. 2018. Preparation of asymmetric phospholipid vesicles for use as cell membrane models. *Nat. Protoc.* 13:2086–2101.
31. Šachl, R., M. Amaro, …, M. Hof. 2015. On multivalent receptor activity of GM1 in cholesterol containing membranes. *Biochim. Biophys. Acta.* 1853:850–857.
32. Amaro, M., R. Šachl, …, M. Hof. 2016. GM1 ganglioside inhibits b-amyloid oligomerization induced by sphingomyelin. *Angew. Chem., Int. Ed. Engl.* 55:9411–9415.
33. Šachl, R., L. B. Johansson, and M. Hof. 2012. Förster resonance energy transfer (FRET) between heterogeneously distributed probes: application to lipid nanodomains and pores. *Int. J. Mol. Sci.* 13:16141–16156.
34. Baumann, J., and M. D. Fayer. 1986. Excitation transfer in dissordered two-dimensional and anisotropic 3-dimensional systems - effects of spatial geometry on time-resolved observables. *J. Chem. Phys.* 85:4087–4107.